Inorganic Chemistry

Article

pubs.acs.org/IC

# Photochemical Dihydrogen Production Using an Analogue of the Active Site of [NiFe] Hydrogenase

Peter A. Summers, Joe Dawson, Fabio Ghiotto, Magnus W. D. Hanson-Heine, Khuong Q. Vuong, E. Stephen Davies, Xue-Z. Sun, Nicholas A. Besley, Jonathan McMaster,* Michael W. George,* and Martin Schröder*

School of Chemistry, University of Nottingham, Nottingham NG7 2RD, United Kingdom

Supporting Information

**ABSTRACT:** Photoproduction of dihydrogen ($H_2$) by a low molecular weight analogue of the active site of [NiFe] hydrogenase has been investigated by reduction of the [$NiFe_2$] cluster, **1**, by a photosensitier PS (PS = [$ReCl(CO)_3(bpy)$] or [$Ru(bpy)_3$][$PF_6$]$_2$). Reductive quenching of the $^3$MLCT excited state of the photosensitizer by $NEt_3$ or $N(CH_2CH_2OH)_3$ (TEOA) generates $PS^{\bullet-}$, and subsequent intermolecular electron transfer to **1** produces the reduced anionic form of **1**. Time-resolved infrared spectroscopy (TRIR) has been used to probe the intermediates throughout the reduction of **1** and subsequent photocatalytic $H_2$ production from [HTEOA][$BF_4$], which was monitored by gas chromatography. Two structural isomers of the reduced form of **1** (**1a**$^{\bullet-}$ and **1b**$^{\bullet-}$) were detected by Fourier transform infrared spectroscopy (FTIR) in both $CH_3CN$ and DMF (dimethylformamide), while only **1a**$^{\bullet-}$ was detected in $CH_2Cl_2$. Structures for these intermediates are proposed from the results of density functional theory calculations and FTIR spectroscopy. **1a**$^{\bullet-}$ is assigned to a similar structure to **1** with six terminal carbonyl ligands, while calculations suggest that in **1b**$^{\bullet-}$ two of the carbonyl groups bridge the Fe centers, consistent with the peak observed at 1714 $cm^{-1}$ in the FTIR spectrum for **1b**$^{\bullet-}$ in $CH_3CN$, assigned to a $\nu$(CO) stretching vibration. Formation of **1a**$^{\bullet-}$ and **1b**$^{\bullet-}$ and production of $H_2$ was studied in $CH_3CN$, DMF, and $CH_2Cl_2$. Although the more catalytically active species (**1a**$^{\bullet-}$ or **1b**$^{\bullet-}$) could not be determined, photocatalysis was observed only in $CH_3CN$ and DMF.

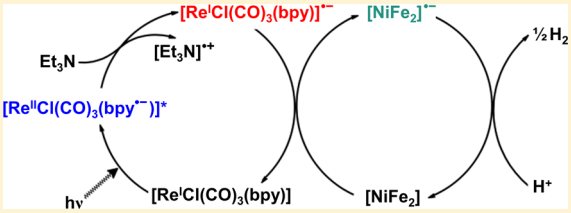


## INTRODUCTION

The development of efficient catalysts for light-driven production of dihydrogen ($H_2$) is a significant challenge for the hydrogen economy,[1] and much attention has focused on generation of efficient catalysts for light-induced splitting of $H_2O$ into $H_2$ and $O_2$.[2] Conversion of $H_2O$ to $H_2$ using solar energy can be a complex, multistep, and multielectron process involving charge separation and bond breaking and formation.[3] Systems containing light-absorbing units, electron relays, and redox catalysts have been targeted to overcome these chemical challenges and led to the development of the three-component system.[4] Traditionally, these systems consist of a photosensitizer, an electron mediator (usually methyl viologen [$MV^{2+}$]), and a homogeneous or heterogeneous metal complex that catalyzes the reduction of protons to $H_2$. In addition, a sacrificial electron donor, such as an amine that may be oxidized readily, injects electrons into the system to complete the catalytic cycle. In recent years, efforts have progressed toward development of a range of homogeneous catalysts containing Co, Pt, Pd, Rh, Fe, and Ni[2a,c,d] centers where the reaction mechanism of proton reduction may be investigated more readily than in heterogeneous catalysts.

The nature of the active sites of the [NiFe] and [FeFe] hydrogenases[5] has inspired synthesis of low molecular weight complexes that mimic the structural, spectroscopic, and functional aspects of these centers[6] and may act as in vitro catalysts for $H_2$ production. While the majority of these compounds have focused on replication of the features of the active sites of the [FeFe] hydrogenases,[7] we focused our attention on preparation of analogues of the active sites of the [NiFe] hydrogenases (Scheme 1);[8] the [NiFe] hydrogenases are $10-10^2$ times less active toward $H_2$ production but show a higher affinity for $H_2$ and are less sensitive to dioxygen and deactivation by CO when compared to their [FeFe] counterparts.[7−9] We reported previously an electrocatalytically active heteronuclear [$NiFe_2$] cluster as an analogue of the active site of the [NiFe] hydrogenases (**1**, Scheme 1).[10] Upon electrochemical reduction of **1** to **1**$^{\bullet-}$ in acidic media, catalytic production of $H_2$ in homogeneous solution occurs with a turnover frequency (TOF) estimated at ca. 6 $h^{-1}$ at a potential of −1.31 V vs $Fc^+$/Fc in $CH_2Cl_2$.[11] The catalytic activity of **1**$^{\bullet-}$ is comparable to those of first-generation analogues of the active site of the [FeFe] hydrogenases but at a potential that is considerably more positive.[12]

Intermolecular electron transfer to analogues of the active sites of the [FeFe] hydrogenases, [$Fe_2(CO)_4X(L^1)(L^2)$], from photogenerated [$Ru(bpy)_3$]$^+$ has been investigated using diethyldithiocarbamate ($dtc^-$) as an electron donor (for X = ($\mu$-$SCH_2$)$_2CH_2$ or ($\mu$-$SCH_2$)$_2NCH_2C_6H_5$, $L^1$ = $L^2$ = CO),[13]

**Received:** January 14, 2014
**Published:** April 22, 2014

   dx.doi.org/10.1021/ic500089b | Inorg. Chem. 2014, 53, 4430−4439

**Scheme 1. (a) Schematic Representation of the Inactive Form of the [NiFe] Hydrogenase (X = $HOO^-$ for Ni−A and $HO^-$ for Ni−B),[7a] (b) 1 ([Ni(L)$Fe_2(Co)_6$], $L^{2-}$ = $(CH_3C_6H_3S_2)_2(CH_2)_3$),[10] and (c) Proposed Mechanism for the Light-Driven Electron Transfer to 1 Using [$ReCl(CO)_3$(bpy)] as a Photosensitiser and $NEt_3$ as a Sacrificial Electron Donor**

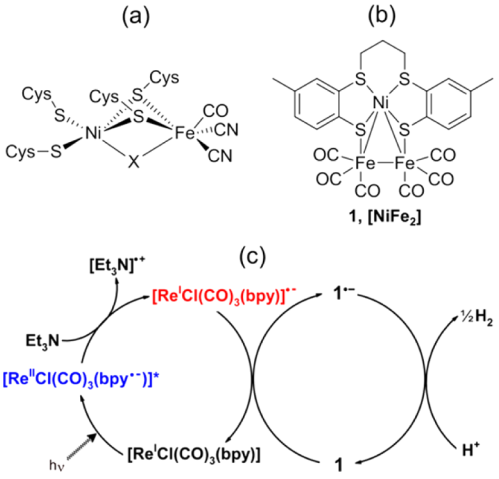


and evolution of $H_2$ occurs when ascorbic acid is used as both electron donor and proton source (for X = $(\mu$-$SCH_2)_2NCH_2C_6H_5$, $L^1 = L^2 = P(Pyr)_3$ or $L^1$ = CO, $L^2 = P(Pyr)_3$, Pyr = *N*-pyrrolyl).[14] Switching to $NEt_3$ as the electron donor and cyclometalated iridium(II) as the photosensitizer leads to a turnover number (TON) of 466 in this system.[15] Ascorbic acid has also been employed as the electron donor and proton source with $[Ru(bpy)_3]^{2+}$ as the photosensitizer in a catalytic system (for X = $\mu$-$Cl_2$bdt, $L^1 = L^2$ = CO, $Cl_2$bdt = 3,6-dichlorobenzene-1,2-dithiolate) that exhibits a TON of 200.[16] Water-soluble $[Fe_2(CO)_4X(L^1)(L^2)]$ (X = $(\mu$-$SCH_2)_2CH_2$, $L^1$ = CO, $L^2$ = a functionalized isonitrile) is catalytically active (TON = 505) when CdTe quantum dots are employed as the photosensitizer and ascorbic acid as a combined electron and proton source.[17] In addition, photocatalytic $H_2$ evolution occurs for $[Fe_2(CO)_6(\mu$-adt$)CH_2C_6H_5]$ or $[Fe_2(CO)_6(\mu$-adt$)$-$C_6H_5]$ [$\mu$-adt = $N(CH_2S)_2$] encapsulated in a dodecyl sulfate micelle in water with [$ReBr(CO)_3$(4,4-dimethylbpy)] and [$ReBr(CO)_3$(1,10-phenanthroline)] as photosensitizers. However, the TON is low for these systems (TON ≤ 0.13).[18] Ni-only catalysts that have been incorporated into $H_2$-evolving systems can demonstrate high TONs.[19] For example, $Ni^{II}$ salts with DHLA (DHLA = dihydrolipoic acid) have been used with CdSe nanocrystals as the photosensitizer to achieve a TON > 600 000 over 360 h of photolysis.[20]

Given the very limited studies of [NiFe]-containing catalysts for $H_2$ production, we report herein detailed studies, including in situ time-resolved spectroscopic analyses, on photoproduction of $H_2$ from the [$NiFe_2$] complex, **1**. Our studies focus on the electron transfer between the photosensitizer, [$ReCl(CO)_3$(bpy)],[21] and **1** with $NEt_3$ or triethanolamine (TEOA) as sacrificial electron donors in $CH_3CN$, DMF, and $CH_2Cl_2$ solutions (Scheme 1). We chose [$ReCl(CO)_3$(bpy)] as the photosensitizer because of its favorable photophysical, electron transfer, and redox properties and because the $\nu$(CO) IR bands of the [$ReCl(CO)_3$(bpy)] unit provide a valuable probe by which the electron transfer can be monitored using time-resolved IR spectroscopy.

## EXPERIMENTAL SECTION

Acetonitrile (99.9%, Merck), $CH_2Cl_2$ (99.9%, Merck), and $NEt_3$ (>99.5%, Sigma-Aldrich) were distilled under an inert atmosphere of Ar from calcium hydride. Dry DMF (99.8%, <0.005% $H_2O$, Arcos) was used as supplied and stored in a glovebox. TEOA (98%, Alfa Aesar) was dried under reduced pressure (160 °C, $1 \times 10^{-1}$ mbar) for 24 h before being stored under Ar. All stock solutions containing TEOA were stored over activated molecular sieves (4 Å) in a glovebox. $CoCp_2$ (Sigma-Aldrich) was sublimed three times and stored in a glovebox. [$^nBu_4N$][$BF_4$] (Sigma-Aldrich) was used as received. [$ReCl(CO)_3$(bpy)],[21] [$Ru(bpy)_3$][$PF_6$]$_2$,[22] [HTEOA][$BF_4$],[23] and **1**[10] were prepared according to literature methods.

**Fourier Transformed Infrared Spectroscopy (FTIR).** FTIR spectra were recorded in solution cells (Harrick Scientific Products, Inc.) with $CaF_2$ windows using a Nicolet 6700 FTIR spectrometer, typically at 2 $cm^{-1}$ resolution. A path length of 0.25, 0.39, 0.5, or 1 mm was used, and all solutions were prepared under an inert atmosphere of Ar and degassed by three freeze−pump−thaw cycles.

**Laser Flash Photolysis.** Nanosecond and picosecond time-resolved infared (TRIR) spectra were obtained using purpose-built equipment based on a pump−probe approach. Details of the equipment and methods used for the TRIR studies have been described previously,[24] a brief description of which is given here. For picosecond experiments the pump beam (400 nm, ca. 150 fs) and tunable probe beam (180 $cm^{-1}$ spectral bandwidth, ca. 150 fs) were generated from a commercial Ti:sapphire oscillator (MaiTai)/regenerative amplifier system (Spitfire Pro, Spectra Physics). For nanosecond experiments the pump beam (355 nm, ca. 600 ps) was provided by a Q-switched Nd:YVO laser (Advanced Optical Technology ACE) and the probe beam was the same as that for the picosecond experiments. In both experiments the mid-IR probe was detected using a 128-element HgCdTe array detector (Infrared Associates) typically with a resolution of ca. 4 $cm^{-1}$. A path length of 0.5 or 1 mm was used, and all solutions for analysis were prepared under an inert atmosphere, degassed by three freeze−pump−thaw cycles, and put under 1.5 atm of Ar.

**Electrochemical Measurements.** Electrochemical measurements were made using an Autolab PGSTAT20 potentiostat. Cyclic voltammograms of 1 mM solutions ($CH_3CN$, DMF, and $CH_2Cl_2$) of each compound in solutions containing [$^nBu_4N$][$BF_4$] (0.2 M in $CH_3CN$ and DMF, 0.4 M in $CH_2Cl_2$) as the supporting electrolyte were recorded using a glassy carbon working electrode, a Pt wire secondary electrode, and a saturated calomel reference electrode at 293 K, unless stated otherwise. Potentials were referenced to the $Fc^{*+}$/Fc* (Fc* = decamethylferrocene) couple used as the internal standard but are reported against the $Fc^+$/Fc couple using an independent calibration under identical conditions. Under these conditions $Fc^{*+}$/Fc* vs $Fc^+$/Fc was −0.498, −0.471, and −0.522 V in $CH_3CN$, DMF, and $CH_2Cl_2$, respectively. Coulometric studies, at a controlled potential, were carried out using a two-compartment cell. The Pt/Rh gauze basket working electrode was separated from the wound Pt/Rh gauze secondary electrode by a glass frit. A saturated calomel reference electrode was bridged to the test solution through a vycor frit orientated at the center of the working electrode. The working electrode compartment was fitted with a magnetic stirrer bar, and the test solution was stirred rapidly during electrolysis.

**$H_2$ Detection.** In a typical experiment [$ReCl(CO)_3$(bpy)] (0.25 mM), **1** (0.05 mM), and TEOA (1 M) in $CH_3CN$ were prepared from thoroughly degassed stock solutions and stored under Ar. Stock solutions containing [$ReCl(CO)_3$(bpy)] and **1** were prepared prior to each experiment and stored in the dark in a glovebox. Ar was continually flowed through the solution and into a 10-port 2-position switch (VICI) at a constant flow (typically 10 $cm^3$ $min^{-1}$), maintained using a mass flow controller (Bronkhorst, E-Flow series). Ar flow was saturated with the reaction solvent before it entered the photolysis cell. A 200 $\mu$L sample was analyzed automatically every 4.5 min using a gas chromatograph (Shimadzu 2014) with a thermal conductivity detector operating at 50 °C. The sample was initially passed through a precolumn (silica) to remove any condensable solvents, which were


dx.doi.org/10.1021/ic500089b | Inorg. Chem. 2014, 53, 4430−4439

subsequently back flushed away to vent prior to the next measurement. Ar was used as the carrier gas, and $H_2$ was detected on an activated molecular sieve column (Shimadzu, CTR-1).

$H_2$ detection was calibrated by dosing the system with known concentrations of $H_2$ using a 6-port 2-position switch (VICI). $H_2$ (Air Products, Premier Plus) at 29.5 psi was used to fill a 5 $\mu$L loop and subsequently switched into the Ar flow (10 $cm^3$ $min^{-1}$) at 14.5 psi. Using the difference in $H_2$ density between the sample loop and the Ar flow at 293 K and the switching repeat time (2−30 s), the molar dosing rate of $H_2$ could be calculated. For low dosing rates (<2.5 × $10^{-8}$ mol $min^{-1}$) 5% $H_2$ in Ar (BOC, Special Gases) was used; the extra Ar was accounted for by a reduction of the Ar flow at the mass flow controller. When $H_2$ was dosed at a constant rate this gave a constant peak area in the chromatogram; varying this flow gave linear fits with the peak area. At a constant $H_2$ flow rate (2.2 × $10^{-8}$ mol $min^{-1}$) the peak area also varied linearly with the Ar flow. Integration of a plot of the production rate versus time yields the total amount of $H_2$ produced.

Irradiation was performed using a Xe arc lamp (Oriel Instruments) operated at 250 W that illuminates an area of 3 $cm^2$. The emitted light was collimated and filtered using a 2.5 cm water filter and a $\lambda$ < 420 nm Pyrex cutoff filter before it illuminates the custom-built cuvette (Helma Analytics, 221-BF).

**DFT Calculations.** Optimized geometries and frequencies were calculated using the Q-Chem quantum-chemical software package.[25] The PBE0 exchange-correlation functional was used[26] together with the triple-$\zeta$-quality Stuttgart relativistic small core pseudopotential and basis set combination for Fe and Ni atoms[27] and the 6-311G(d) basis set for atoms H, C, O, and S.[28] The default SG-1 numerical integration grid was used for evaluation of the exchange-correlation energy in order to make the calculations more computationally tractable.[29] [$NiFe_2$] ([$Ni(L)Fe_2(CO)_6$]) models were constructed using the unmethylated [$NiFe_2$] analogue $L^{2-}$ = $(C_6H_4S_2)_2(CH_2)_3$, as opposed to $L^{2-}$ = $(CH_3C_6H_3S_2)_2(CH_2)_3$, in order to reduce the computational time. The initial molecular structures for the neutral and anionic species of the model [$NiFe_2$] complex were optimized to minimum energy geometries using tightened energy convergence criteria of 1 × $10^{-7}$ $E_h$ and a gradient convergence of 1 × $10^{-6}$ $E_h a_0^{-1}$. Harmonic frequencies were obtained by adding numerical second derivatives of the nuclear energy with respect to displacement, calculated by finite difference of the analytical gradient (0.00189 $a_0$ step size) to analytical second derivatives of the electronic energy. The resulting harmonic frequencies were scaled by a uniform factor of 1.011 determined by least-squares fitting.[30] Calculations involving the neutral and anionic species were performed using restricted and unrestricted DFT, respectively.

## RESULTS AND DISCUSION

**Photoinduced Electron Transfer between $NEt_3$, [$ReCl(CO)_3$(bpy)], and 1 in $CH_3CN$.** *TRIR Spectroscopy.* We used fast time-resolved infrared spectroscopy (TRIR), a combination of flash photolysis with fast IR detection,[31] to monitor the proposed transient species involved in the generation of $\mathbf{1}^{\bullet-}$ in Scheme 1 in $CH_3CN$. The photophysics of **1** (1 mM) was investigated using TRIR in $CH_3CN$. Irradiation at 355 nm produces a short-lived transient observed at time delays < 1 ns with IR bands that are red shifted relative to the parent (2025, 1988, and 1942 $cm^{-1}$), and these bands rapidly recombine to form those of **1** with a lifetime of ca. 90 ps (Figure S1, Supporting Information). These results are similar to recently reported TRIR results for $Fe_3(CO)_{12}$, which show a similar short-lived transient associated with homolysis of at least one of the FeFe bonds.[32] Following the reformation of **1** there are no more observable photoproducts on the nanosecond time scale. Thus, subsequent TRIR investigations are not complicated by the intrinsic photochemistry of **1**.

To investigate whether addition of [$ReCl(CO)_3$(bpy)] and $NEt_3$ affects the photochemistry of **1**, the TRIR experiment was repeated in the presence of [$ReCl(CO)_3$(bpy)] and $NEt_3$. The FTIR spectrum of **1** (0.76 mM) and [$ReCl(CO)_3$(bpy)] (0.75 mM) in a solution of $NEt_3$ (1 M) and $CH_3CN$ (Figure 1a)

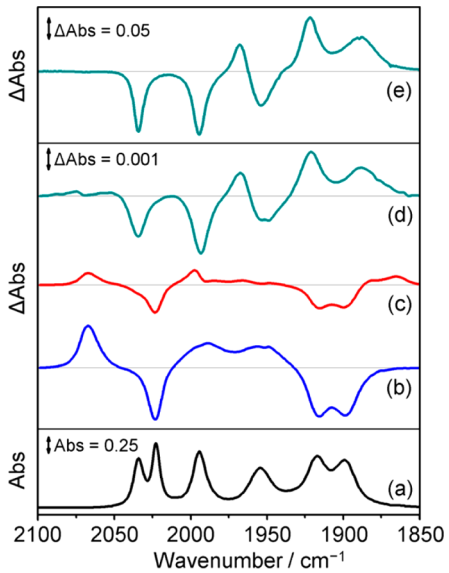


**Figure 1.** FTIR and TRIR spectra of **1** (0.76 mM) and [$ReCl(CO)_3$(bpy)] (0.75 mM) in a solution of $CH_3CN$ and $NEt_3$ (1 M). (a) FTIR ground state spectrum. TRIR difference spectra (b) 1.5, (c) 20, and (d) 500 ns after flash photolysis at 355 nm. (e) FTIR difference spectrum obtained 5 s after 30 s irradiation of an identical solution using a LED white light source and a $\lambda$ < 420 nm cutoff filter.

possesses 6 carbonyl bands; the bands at 2035, 1994, and 1955 $cm^{-1}$ are assigned to **1**, and the bands at 2023, 1917, and 1900 $cm^{-1}$ are associated with [$ReCl(CO)_3$(bpy)]. The IR spectrum taken 1.5 ns after photolysis at 355 nm only shows bleaching of the bands assigned to [$ReCl(CO)_3$(bpy)], and transient $\nu$(CO) peaks are observed at 2068, 1989, and 1954 $cm^{-1}$ (Figure 1b). These new bands are shifted to higher energy relative to those of the parent [$ReCl(CO)_3$(bpy)] complex, consistent with formation of the $^3$MLCT excited state, [$ReCl(CO)_3$(bpy)]*.[33] At this early time there is no change in the intensity and energies of the bands associated with the [$NiFe_2$] cluster, **1**. In the presence of $NEt_3$, [$ReCl(CO)_3$(bpy)]* is reductively quenched to form the one-electron-reduced photosensitizer $[ReCl(CO)_3(bpy)]^{\bullet-}$ (1997, 1880, and 1864 $cm^{-1}$) such that the TRIR spectrum obtained at 20 ns is dominated by this one-electron-reduced species (Figure 1c).[34] $[ReCl(CO)_3(bpy)]^{\bullet-}$ is stable for >1 s in the absence of an oxidant in solution, but in the presence of **1** $[ReCl(CO)_3(bpy)]^{\bullet-}$ reacts rapidly on the nanosecond time scale with concomitant bleaching of the $\nu$(CO) bands of **1** and formation of a new species with bands at 1968, 1921, and 1890 $cm^{-1}$ (Figure 1d). This new species can be assigned to formation of the one-electron-reduced form of **1**, $\mathbf{1a}^{\bullet-}$, by comparison with IR spectra derived from spectroelectrochemical experiments; in addition, electrochemical experiments show a broad band at 1779 $cm^{-1}$ associated with $\mathbf{1a}^{\bullet-}$ but which falls outside the spectral window of the TRIR study.[10] Another isomer of the reduced form of **1**, $\mathbf{1b}^{\bullet-}$, can be detected under certain conditions. Proposed structures for both $\mathbf{1a}^{\bullet-}$ and $\mathbf{1b}^{\bullet-}$ are discussed later in the text.


dx.doi.org/10.1021/ic500089b | Inorg. Chem. 2014, 53, 4430−4439

Quenching of the $^3$MLCT state of [ReCl(CO)$_3$(bpy)]* can be clearly evaluated in the TRIR kinetics of the electron transfer process, obtained via multiple band fitting of the TRIR spectra (Figure 2).

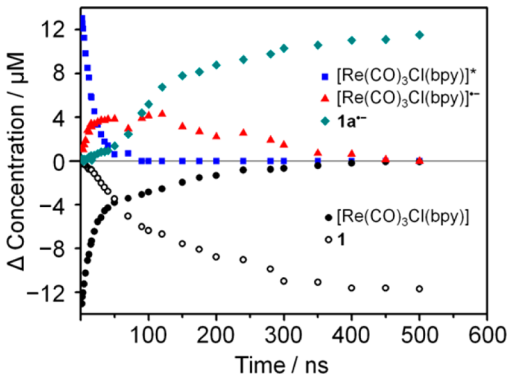


**Figure 2.** TRIR kinetic traces for the decay of the $^3$MLCT excited state [ReCl(CO)$_3$(bpy)]* (blue squares), growth and decay of [ReCl(CO)$_3$(bpy)]$^{\bullet-}$ (red triangles), growth of **1a**$^{\bullet-}$ (green diamonds), regeneration of [ReCl(CO)$_3$(bpy)] (black dots), and loss of **1** (circles) recorded in $CH_3CN$ following flash photolysis (355 nm) of **1** (0.76 mM) and [ReCl(CO)$_3$(bpy)] (0.75 mM) in a solution of $NEt_3$ (1 M) and $CH_3CN$.

Assuming that formation of [ReCl(CO)$_3$(bpy)]* and subsequent growth of **1a**$^{\bullet-}$ are the only significant processes that occur and that these are represented by the loss of [ReCl(CO)$_3$(bpy)] and **1**, respectively, then the band areas can be used to estimate the concentrations of each species in solution. The $^3$MLCT state in [ReCl(CO)$_3$(bpy)]* is formed within the time scale of these experiments and decays with a lifetime of 17 (±0.3) ns (Figures 2 and S2, blue squares, Supporting Information) and is accompanied by reformation of [ReCl(CO)$_3$(bpy)] (Figure 2, black dots). This parent regrowth occurs through two processes, the first of which (representing ca. 70% of the regrowth) is associated with relaxation of [ReCl(CO)$_3$(bpy)]* → [ReCl(CO)$_3$(bpy)]. Simultaneously, growth of [ReCl(CO)$_3$(bpy)]$^{\bullet-}$ is observed (Figure 2, red triangles) and on longer time scales (50−500 ns). [ReCl(CO)$_3$(bpy)]$^{\bullet-}$ reduces **1**, and the remaining [ReCl(CO)$_3$(bpy)] is recovered, which accounts for the remaining 30% of the regrowth of [ReCl(CO)$_3$(bpy)]. **1** is lost (Figure 2, circles) and **1a**$^{\bullet-}$ is formed (Figure 2, green diamonds) such that the IR spectrum obtained at 500 ns is dominated by **1a**$^{\bullet-}$. The sigmoidal growth of **1a**$^{\bullet-}$ is consistent with its formation from an intermediate species, namely, [ReCl(CO)$_3$(bpy)]$^{\bullet-}$ (Scheme 1). Thus, electron transfer from [ReCl(CO)$_3$(bpy)]$^{\bullet-}$ to **1** forms **1a**$^{\bullet-}$, which remains stable on the time scale of this experiment (up to 0.1 ms). On the basis of our TRIR spectroscopic results, we estimate the second-order rate constant, $k_{inter}$, for electron transfer between [ReCl(CO)$_3$(bpy)]$^{\bullet-}$ and **1** as $k_{inter} = 6.7 \times 10^9$ M$^{-1}$ s$^{-1}$ (Figure S2, Supporting Information). Control experiments involving irradiation of a solution of **1** and [ReCl(CO)$_3$(bpy)] in

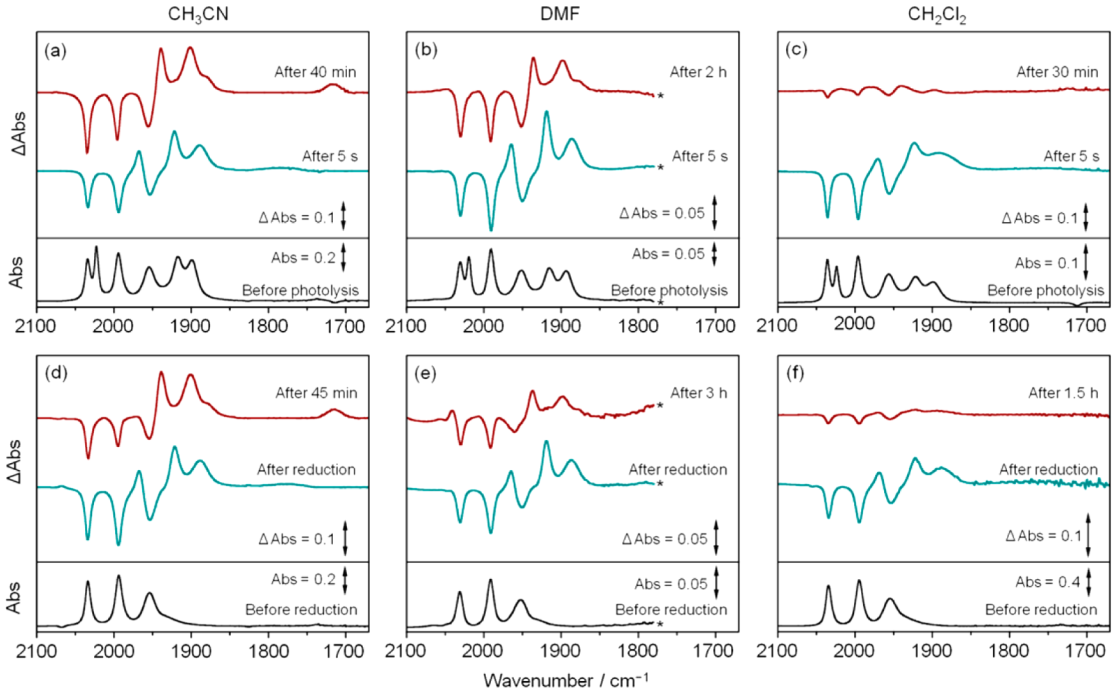


**Figure 3.** FTIR spectra comparing the photochemical (top row, a, b, and c) and electrochemical (bottom row, d, e, and f) reduction of **1** to **1a**$^{\bullet-}$ and **1b**$^{\bullet-}$. (Top row) FTIR ground state spectra of **1** (1 mM) and [ReCl(CO)$_3$(bpy)] (1 mM) in a solution of $NEt_3$ (1 M) and $CH_3CN$ (a), DMF (b), and $CH_2Cl_2$ (c) (black lines). FTIR difference spectra of **1a**$^{\bullet-}$ 5 s after photochemical reduction (between 20 and 30 s photolysis time) according to Scheme 1 (green lines). FTIR difference spectra of **1b**$^{\bullet-}$ 40 min after photolysis in $CH_3CN$, 2 h after photolysis in DMF, and 30 min after photolysis in $CH_2Cl_2$ (brown lines in a, b, and c, respectively). (Bottom row) FTIR ground state spectra of **1** (1 mM) in a solution in $CH_3CN$ (a), DMF (b), and $CH_2Cl_2$ (c) containing [$^n$Bu$_4$N][BF$_4$] (0.2 M in $CH_3CN$ and DMF, 0.4 M in $CH_2Cl_2$) as supporting electrolyte (black lines). FTIR difference spectra of **1a**$^{\bullet-}$ after electrochemical reduction in $CH_3CN$ (d), DMF (e), and $CH_2Cl_2$ (f) (green lines). FTIR difference spectra of **1b**$^{\bullet-}$ 45 min after reduction in $CH_3CN$, 3 h after reduction in DMF, and 1.5 h after reduction in $CH_2Cl_2$ (brown lines in d, e, and f, respectively). To facilitate comparison with the photochemical experiments, spectra for electrochemically generated **1b**$^{\bullet-}$ in $CH_3CN$ and DMF are generated through the partial spectral subtraction of **1a**$^{\bullet-}$. Solvent bands of DMF are omitted for clarity.


dx.doi.org/10.1021/ic500089b | Inorg. Chem. 2014, 53, 4430−4439

$CH_3CN$ show no direct interaction between **1** and the excited state of the photosensitizer; under these conditions the presence of $\mathbf{1a}^{\bullet-}$ was not observed.

The upper limits of the concentration of $\mathbf{1a}^{\bullet-}$ and $[ReCl(CO)_3(bpy)]^{\bullet-}$ are estimated as ca. 11 and ca. 5 $\mu$M, respectively (Figure 2), suggesting that the concentration of $\mathbf{1a}^{\bullet-}$ reaches a value ca. double of that of $[ReCl(CO)_3(bpy)]^{\bullet-}$. However, according to Scheme 1, the maximum concentration for $\mathbf{1a}^{\bullet-}$ and $[ReCl(CO)_3(bpy)]^{\bullet-}$ would be expected to have a value that was approximately equivalent. Reductive quenching of the $^3$MLCT excited state of $[ReCl(CO)_3(bpy)]$ by $NEt_3$ results in formation of a N-centered radical cation, $^{\bullet}NEt_3^+$, and this species could generate a second reducing equivalent through a thermal dark process. Thus, extraction of $H^{\bullet}$ from another molecule of $NEt_3$ by $^{\bullet}NEt_3^+$ may result in formation of $HNEt_3^+$ and a strongly reducing C-centered radical, $CH_3C^{\bullet}HNEt_2$.[35] By analogy with the chemistry of radical cations formed from TEOA,[36] $CH_3C^{\bullet}HNEt_2$ could reduce either $[ReCl(CO)_3(bpy)]$ or **1** and ultimately generate a second equivalent of $\mathbf{1a}^{\bullet-}$.[35,37] Similar decomposition reactions have been proposed previously for TEOA and $NEt_3$ on oxidation.[38] Indeed, decomposition of $TEOA^{\bullet+}$ has been proposed to reduce $[ReX(CO)_3(bpy)]$ (X = Cl, Br) in DMF.[36,39] In addition, alkyl radicals of $NEt_3$ have also been identified by spin trapping following continuous irradiation of $NEt_3$ and Ru(II) polypyridyl complexes in DMF.[35]

**Photoinduced Electron Transfer between $NEt_3$, $[ReCl(CO)_3(bpy)]$, and 1 in $CH_3CN$, DMF, and $CH_2Cl_2$.** *FTIR Spectroscopy.* Formation of $\mathbf{1a}^{\bullet-}$ was probed by FTIR spectroscopy using white light irradiation from a visible LED light source (20−30 s with a $\lambda$ < 420 nm Pyrex cutoff filter) under Ar. The FTIR spectrum of **1** (1 mM) and $[ReCl(CO)_3(bpy)]$ (1 mM) in a solution of $NEt_3$ (1 M) and $CH_3CN$ obtained 5 s after photolysis (Figures 3a and 1e, green lines) clearly shows the presence of bands assigned to $\mathbf{1a}^{\bullet-}$ and is identical to the TRIR spectra obtained after 500 ns (Figure 1d).[10] There are no significant changes in the bands associated with the photosensitizer, consistent with its regeneration in the catalytic cycle (Scheme 1). Control experiments, in which either $NEt_3$ or $[ReCl(CO)_3(bpy)]$ was absent from the test solution, lead to no significant changes in the IR spectrum after photolysis. Thus, $[ReCl(CO)_3(bpy)]$, **1**, and $NEt_3$ are all necessary for the complete electron transfer cycle.

Photocatalytic production of $\mathbf{1a}^{\bullet-}$ from **1** also occurs in DMF and $CH_2Cl_2$ solutions (Figure 3b and 3c, green lines). Once formed, however, $\mathbf{1a}^{\bullet-}$ is not stable but undergoes subsequent transformations over time scales of up to 3 h depending on the nature of the solvent. In $CH_3CN$ and DMF solutions the bands associated with the parent bleach remain constant while those of $\mathbf{1a}^{\bullet-}$ decrease in intensity. Formation of a new product with $\nu$(CO) bands at 1992, 1939, 1901, 1880, and 1714 $cm^{-1}$ in $CH_3CN$ and 1989, 1936, 1898, and 1878 $cm^{-1}$ in DMF is observed (Figure 3a and 3b after 40 min and 2 h, respectively, brown lines). The red shift (ca. 50 $cm^{-1}$) of the band positions of this new product relative to those of **1**, together with electrochemical data (see below), have led to the assignment of this new species, $\mathbf{1b}^{\bullet-}$, as an overall one-electron-reduced product of **1** at the same oxidation state level as $\mathbf{1a}^{\bullet-}$. The band at 1714 $cm^{-1}$ in $CH_3CN$ solution suggests formation of a bridging metal carbonyl species; this band is not observed in DMF due to strong solvent absorbance in this region (Figure 3b, brown line). In $CH_2Cl_2$ solution the bands associated with $\mathbf{1a}^{\bullet-}$ decrease in intensity and are accompanied by regrowth of bands for **1** such that the difference spectrum (Figure 3c, brown line) 1.5 h after photolysis shows only weak negative features associated with **1** and weak positive features at ca. 1980, 1941, and 1898 $cm^{-1}$. The bands at 1941 and 1980 $cm^{-1}$ could indicate formation of a small quantity of $\mathbf{1b}^{\bullet-}$ in $CH_2Cl_2$. However, due to the weak intensity of these bands further investigation is required to unequivocally determine their origin.

We probed the formation of $\mathbf{1b}^{\bullet-}$ from $\mathbf{1a}^{\bullet-}$ by electrochemical and chemical reduction of **1** in $CH_3CN$, DMF, and $CH_2Cl_2$ solutions. The cyclic voltammetry of **1** shows a reduction process at $E_{1/2}$ = −1.20, −1.19, and −1.29 V vs $Fc^+$/Fc in $CH_3CN$, DMF, and $CH_2Cl_2$, respectively (Figure S4, Supporting Information), which is electrochemically reversible in all three solvents and consistent with reported values in $CH_2Cl_2$ ($E_{1/2}$ = −1.31 V vs $Fc^+$/Fc).[10] The reduction process in $CH_3CN$, DMF, and $CH_2Cl_2$ solutions was investigated by monitoring the FTIR spectrum of **1** after electrochemical reduction. In $CH_2Cl_2$ solution, the electrochemical reduction of **1** at −1.54 V vs $Fc^+$/Fc results in formation of $\mathbf{1a}^{\bullet-}$, which is oxidized back to **1** over 1.5 h, presumably by the ingress of dioxygen (Figure 3f, brown line). In $CH_3CN$ and DMF solutions electrochemical reduction of **1** at −1.42 and −1.49 V vs $Fc^+$/Fc, repectively, also results in formation of $\mathbf{1a}^{\bullet-}$, which subsequently converts to $\mathbf{1b}^{\bullet-}$ (Figure 3d and 3e, brown lines) as observed in the photochemical reactions (Figure 3a and 3b, brown lines). Cyclic voltammograms recorded on the solutions after reduction (45 min in $CH_3CN$ and 3 h in DMF) show an oxidation process at $E_p^a$ = −0.59 and −0.52 V vs $Fc^+$/Fc in $CH_3CN$ and DMF, respectively, associated with the presence of $\mathbf{1b}^{\bullet-}$ (Figure 4). This new process, assigned to oxidation of $\mathbf{1b}^{\bullet-}$, has a small associated reduction process at $E_p^c$ = −0.73 V vs $Fc^+$/Fc in $CH_3CN$. In DMF no associated reduction process was observed (Figure 4b); however, the cathodic current associated with conversion of **1** to $\mathbf{1a}^{\bullet-}$ is increased ($E_p^c$ =

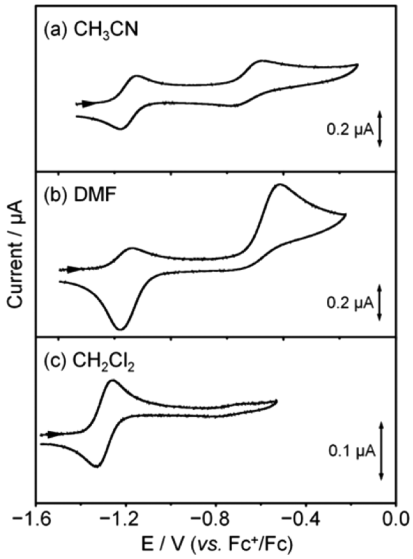


**Figure 4.** Cyclic voltammograms following bulk reduction of **1** in (a) $CH_3CN$ ($\mathbf{1a}^{\bullet-}$ and $\mathbf{1b}^{\bullet-}$ in solution after ca. 45 min), (b) DMF ($\mathbf{1a}^{\bullet-}$ and $\mathbf{1b}^{\bullet-}$ in solution after ca. 3 h), and (c) $CH_2Cl_2$ ($\mathbf{1a}^{\bullet-}$ and **1** in solution) at 298 K containing $[^nBu_4N][BF_4]$ (0.2 M in $CH_3CN$ and DMF, 0.4 M in $CH_2Cl_2$) as a supporting electrolyte at a scan rate of 100 mV $s^{-1}$.


dx.doi.org/10.1021/ic500089b | Inorg. Chem. 2014, 53, 4430−4439

−1.23 V vs $Fc^+/Fc$), suggesting that oxidation of $\mathbf{1b}^{\bullet-}$ has reformed **1**.

Chemical reduction of **1** by $CoCp_2$ ($Cp^-$ = cyclopentadienyl) generates $\mathbf{1a}^{\bullet-}$ in $CH_3CN$ and DMF solutions, which then converts to $\mathbf{1b}^{\bullet-}$. Growth of $\mathbf{1b}^{\bullet-}$ in $CH_3CN$ and DMF solution follows a first-order process with lifetimes of 516 (±6) and 6360 (±100) s [$k_{ab}$ = 19.4 (±0.2) and 1.57 (±0.02) × $10^{-4}$ $s^{-1}$] in $CH_3CN$ and DMF, respectively (Figure 5d, brown dots). These results and the first-order nature of the process suggest that the species $\mathbf{1b}^{\bullet-}$ is not formed from a dimer produced from two $\mathbf{1a}^{\bullet-}$ molecules, a process that has been observed following reduction of ($\mu$-pdt)[$Fe(CO)_3$]$_2$ ($pdt^{2-}$ = $^-S(CH_2)_3S^-$).[40] In $CH_3CN$ solution, unassigned bands at 2013, 1977, and 1932 $cm^{-1}$ are also observed as a secondary product, consistent with the decay of $\mathbf{1a}^{\bullet-}$ fitting to a biexponential fit with time constants 420 (±5) and 2520 (±50) s and pre-exponential factors 0.543 (±0.005) and 0.453 (±0.004) (Figure 5d), where the time constant 420 (±5) s is associated with formation of $\mathbf{1b}^{\bullet-}$. Formation of $\mathbf{1b}^{\bullet-}$ is not accompanied by growth of any other peaks in the $\nu$(CO) region of the IR spectrum in DMF solution.

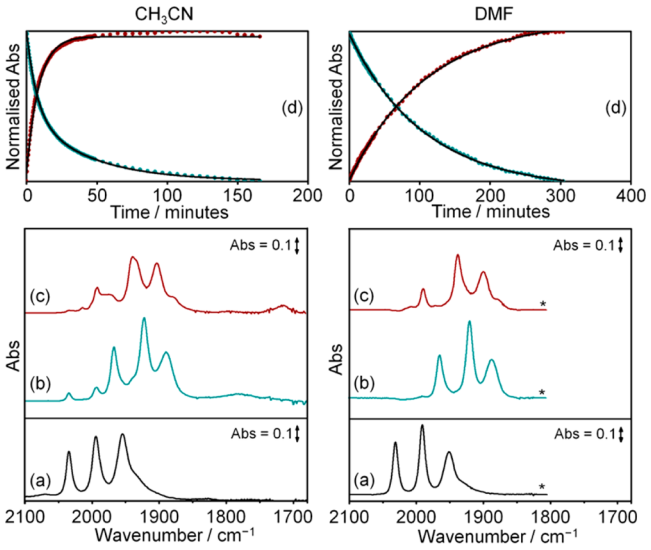


**Figure 5.** FTIR spectra of $\mathbf{1a}^{\bullet-}$ and $\mathbf{1b}^{\bullet-}$ generated after chemical reduction of **1** with $CoCp_2$ in $CH_3CN$ (left) and DMF (right). (a) FTIR ground state spectra of **1** (2 mM). (b) FTIR spectra of $\mathbf{1a}^{\bullet-}$ 5 s following chemical reduction with $CoCp_2$ (2 and 2.1 mM in $CH_3CN$ and DMF, respectively). (b) FTIR spectra after thermal formation of $\mathbf{1b}^{\bullet-}$ in $CH_3CN$ (ca. 150 min) and DMF (ca. 5 h). (d) Single-point kinetic trace following conversion of $\mathbf{1a}^{\bullet-}$ to $\mathbf{1b}^{\bullet-}$, 1967 (green dots) and 1991 (brown dots) $cm^{-1}$ in $CH_3CN$, 1964 (green dots) and 1988 (brown dots) $cm^{-1}$ in DMF. (*) Solvent bands of DMF omitted for clarity.

After chemical generation of $\mathbf{1b}^{\bullet-}$ from **1** using $CoCp_2$ in $CH_3CN$, removal of $CH_3CN$ under reduced pressure followed by addition of $CH_2Cl_2$ results in **1** being observed in the FTIR spectrum. Thus, **1** appears to form via back-electron transfer to $[CoCp_2]^+$ in $CH_2Cl_2$ solution. This would suggest that $\mathbf{1b}^{\bullet-}$ is not a decomposition product from $\mathbf{1a}^{\bullet-}$ and must be closely linked structurally to **1**. Once formed $\mathbf{1b}^{\bullet-}$ slowly decomposes over ca. 8 h without growth of any clearly observable new metal carbonyl bands.

*DFT Calculations.* We performed density functional theory (DFT) geometry optimizations and harmonic frequency calculations to provide theoretical models for **1** and its reduced forms, $\mathbf{1a}^{\bullet-}$ and $\mathbf{1b}^{\bullet-}$. We were able to determine two minimum energy geometries for the one-electron-reduced state and one for the neutral species. The geometries for the experimental and calculated frequencies and the experimental FTIR spectra of **1**, $\mathbf{1a}^{\bullet-}$, and $\mathbf{1b}^{\bullet-}$ are shown in Table 1 and Figure 6. The atom-labeling schemes for **1**, $\mathbf{1a}^{\bullet-}$, and $\mathbf{1b}^{\bullet-}$ are shown in Figures S5−S8, Supporting Information.

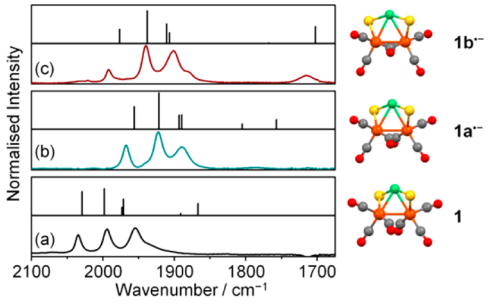


**Figure 6.** Calculated scaled harmonic vibrational frequencies above the experimental $\nu$(CO) data as observed by FTIR in $CH_3CN$ (left). Predicted geometries of the $Fe_2$ coordination sphere (right) for models of the [$NiFe_2$] cluster in the neutral and two separate reduced forms, **1** (a), $\mathbf{1a}^{\bullet-}$ (b), and $\mathbf{1b}^{\bullet-}$ (c).

The DFT calculations of **1** reproduce the principal features of the experimental geometry of **1** including the nonplanarity of the $NiS_4$ unit; the dihedral angle between the planes defined by atoms S(1)−Ni−S(2) and S(3)−Ni−S(4) (85.3°) is in close agreement with the dihedral angle reported for the crystal structure (85.7°).[10] The Ni−S(thiolate), Ni−S(thioether), and Fe−S bonds are ca. 0.05, 0.1, and 0.05 Å longer, respectively, than the corresponding experimental distances in **1**. A comparison of the experimental and calculated Fe−C distances for the CO ligands defined by C(3) and C(4) (Table 1) predicts a greater degree of semibridging character in the gas-phase structure. These differences between the calculated gas-phase geometry and the X-ray crystal structure of **1** are similar to those reported previously for DFT calculations for **1** that employed the BP86 functional.[10] Thus, while the calculations

**Table 1. Photochemical FTIR $\nu$(CO) Data in $CH_3CN$, $CH_2Cl_2$, and DMF and Scaled Harmonic Frequencies of Species Relating to 1**

| | $\nu$(CO)/$cm^{-1}$ | | | |
|---|---|---|---|---|
| | **1** | $\mathbf{1a}^{\bullet-}$ | $\mathbf{1b}^{\bullet-}$ | ref |
| $CH_3CN$ | 2035, 1994, 1955, 1936 (w, sh) | 1968, 1921, 1890, 1779 (w, br) | 1992, 1939, 1901, 1880, 1714 | this work |
| DMF | 2031, 1991, 1952, 1936 (w, sh) | 1965, 1919, 1887, 1773 (w, br) | 1989, 1936, 1898, 1878 | this work |
| $CH_2Cl_2$ | 2036, 1996, 1956, 1936 (w, sh) | 1967, 1923, 1891, 1758 (w, br) | not observed | ref 10; this work |
| calculated | 2029, 1998, 1973, 1971, 1891, 1867 | 1956, 1921, 1893, 1890, 1805, 1757 | 1976, 1938, 1911, 1906, 1768 (w), 1702 | this work |


dx.doi.org/10.1021/ic500089b | Inorg. Chem. 2014, 53, 4430−4439

reproduce the principal features of the bonding, we note that differences between the calculated and the experimental $\nu$(CO) (see below) may reflect the greater semibridging character of the CO ligands defined by atoms C(3) and C(4) in the calculated gas-phase structure relative to the experimental geometry.

The calculated geometry of $\mathbf{1a}^{\bullet-}$ is very similar to that calculated for **1** and is, therefore, entirely consistent with previous assignments of the one-electron-reduced [$NiFe_2$] species.[10] The changes to the overall structure include the lowering of the approximate $C_2$ symmetry brought about by an elongation of the Ni−S(2) bond by 0.15 Å compared with 0.04 Å for the Ni−S(4) bond, a 0.20 Å elongation of both Ni−Fe bonds, and a minor increase in the asymmetry and apparent semibridging character predicted for the C(3)O(3) and C(4)O(4) carbonyl groups [Fe(1)−C(3) = 1.83 Å, Fe(2)−C(4) = 1.80 Å, Fe(1)−C(4) = 2.25 Å, and Fe(2)−C(3) = 2.14 Å for $\mathbf{1a}^{\bullet-}$]. In contrast, on moving from $\mathbf{1a}^{\bullet-}$ to $\mathbf{1b}^{\bullet-}$ there is a dramatic rearrangement from semibridging to almost complete bridging character for the C(3)O(3) and C(4)O(4) ligands. The Fe−C bond lengths for the two ligands elongate by 0.08 and 0.11 Å for the Fe(1)−C(3) and Fe(2)−C(4) bonds, respectively, as they move to a more symmetric bridging mode. The distance between the two Fe centers also decreases by 0.05 Å, and the dihedral angle between the planes defined by C(3)−Fe(1)−Fe(2) and C(4)−Fe(1)−Fe(2) reduces from 51 to 31°, increasing the planarity of the two bridging CO groups.

Theoretical infrared spectra and frequencies (1.011 scaling factor, Figure 6 and Table 1) for **1**, $\mathbf{1a}^{\bullet-}$, and $\mathbf{1b}^{\bullet-}$ provide a qualitative match for the experimental spectra of **1**, $\mathbf{1a}^{\bullet-}$, and $\mathbf{1b}^{\bullet-}$ in $CH_3CN$ solution and importantly reproduce the key features in each spectrum including the frequency downshift on reduction of **1** to $\mathbf{1a}^{\bullet-}$ observed for all three CO bands. Similarly, the frequency increase in the CO bands of $\mathbf{1b}^{\bullet-}$ relative to $\mathbf{1a}^{\bullet-}$ is reproduced with scaled harmonic bands moving to 1976, 1938, and 1911 $cm^{-1}$ for $\mathbf{1b}^{\bullet-}$.

The most significant spectral feature in the experimental IR spectrum of $\mathbf{1b}^{\bullet-}$ in $CH_3CN$ solution is the presence of a single infrared band at 1714 $cm^{-1}$ (Figures 3a and 6c and Table 1), which is absent from the spectra of **1** and $\mathbf{1a}^{\bullet-}$. DFT calculations of **1** and $\mathbf{1a}^{\bullet-}$ show semibridging CO stretches at 1867 and 1891 $cm^{-1}$ and at 1757 and 1805 $cm^{-1}$, respectively. These bands reflect a potential overestimation of CO bridging character in **1** but match the broad experimental peak seen at 1779 $cm^{-1}$ for $\mathbf{1a}^{\bullet-}$ in $CH_3CN$ solution. The calculated spectrum of $\mathbf{1b}^{\bullet-}$ shows a single intense infrared peak in the carbonyl bridging region at 1702 $cm^{-1}$ (Figure 6c, Table 1). Thus, the presence of a single low-energy intense infrared band in the experimental and calculated IR spectra of $\mathbf{1b}^{\bullet-}$ and the qualitative match between the calculated and the experimental infrared bands for **1** and $\mathbf{1a}^{\bullet-}$ together with the similarities between the calculated structure for **1** and the experimentally determined structure support the assignment of the $\mathbf{1b}^{\bullet-}$ calculated structure as a model of the second one-electron reduction product of **1**.

**Photoinduced Electron Transfer between $NEt_3$, [Ru(bpy)$_3$][$PF_6$]$_2$, and 1 in $CH_3CN$.** *TRIR and FTIR Spectroscopies.* $[Ru(bpy)_3]^{2+}$ has been used extensively as a photosensitizer for photoinduced $H_2$ production and chemical reactions.[2d,41] Although $[Ru(bpy)_3]^{2+}$ does not possess a convenient IR probe [e.g., $\nu$(CO) bands], electron transfer to **1** can be monitored in the $\nu$(CO) region of the IR spectrum via growth of $\mathbf{1a}^{\bullet-}$. The FTIR spectrum of **1** (1 mM) and $[Ru(bpy)_3][PF_6]_2$ (1 mM) in a solution of $CH_3CN$ and $NEt_3$ (1.5 M) possesses three bands originating from **1** (Figure S3(a), Supporting Information). At 1.5 ns following excitation of the sample, there is no significant change in the $\nu$(CO) bands of **1** in the TRIR spectrum (Figure S3(b), Supporting Information). Over the subsequent 500 ns, the parent peaks of **1** are observed to deplete as new bands grow in that are associated with formation of $\mathbf{1a}^{\bullet-}$ (Figure S3(c), Supporting Information). Single-point kinetic traces recorded for **1** and $\mathbf{1a}^{\bullet-}$ at 1955 and 1926 $cm^{-1}$, respectively (Figure S3(e), Supporting Information), show sigmoidal growth and decay that are similar to that recorded in the experiments described above using [$ReCl(CO)_3$(bpy)] as the photosensitizer (Figure 2). This suggests that the mechanism of reduction is comparable to that of Scheme 1 and proceeds via reductive quenching of $[Ru(bpy)_3]^{2+*}$ to form $[Ru(bpy)_3]^{+}$. Formation of $\mathbf{1a}^{\bullet-}$ occurs on a time scale comparable to that of [$ReCl(CO)_3$(bpy)], up to 500 ns (Figures 2 and S3(e), Supporting Information) ,suggesting that $k_{inter}$ is comparable in each case.

*$H_2$ Production.* Our TRIR, photochemical, chemical, and electrochemical studies clearly identify the species involved in the photochemical generation of $\mathbf{1a}^{\bullet-}$ and $\mathbf{1b}^{\bullet-}$ from **1** using [$ReCl(CO)_3$(bpy)] as a photosensitizer and $NEt_3$ as a sacrificial electron donor. In order to investigate the photochemical production of $H_2$, we used a mixture of TEOA (1 M) and [HTEOA][$BF_4$] (0.1 M) as a combined sacrificial electron donor and proton source in place of $NEt_3$. $H_2$ production was monitored during continuous irradiation of **1** (0.05 mM), [$ReCl(CO)_3$(bpy)] (0.25 mM), TEOA (1 M), and [HTEOA][$BF_4$] (0.1 M) in degassed $CH_3CN$ (Figure 7a). After an initial induction period (ca. 5 min), the rate of $H_2$ production is linear over ca. 22 min (13.0 $\mu$mol $h^{-1}$, TOF = 52 $h^{-1}$) before $H_2$ production decreases to reach a plateau after ca. 3 h (13.8 $\mu$mol, TON = 55, Figure 7a, red dots). After photolysis a fine black precipitate could be observed in solution, the role of which in catalysis cannot be excluded. Removal of the proton source, [HTEOA][$BF_4$], from the reaction mixture results in an

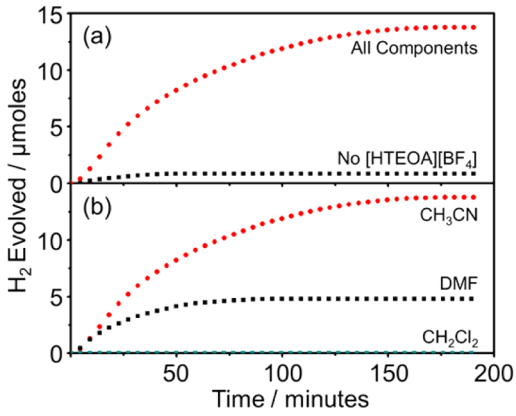


**Figure 7.** (a) Time-dependent photoinduced $H_2$ evolution from a 5 mL degassed solution containing **1** (0.05 mM), [$ReCl(CO)_3$(bpy)] (0.25 mM), TEOA (1 M), and [HTEOA][$BF_4$] (0.1 M) in $CH_3CN$ at 293 K (red dots). Control experiment in the absence of [HTEOA][$BF_4$] from the reaction mixture (black squares). (b) Time-dependent photoinduced $H_2$ evolution carried out at the same concentration as in a in $CH_3CN$ (red dots), DMF (black squares), and $CH_2Cl_2$ (green squares) solutions. Irradiation was performed using a Xe lamp (250 W) and a $\lambda$ < 420 nm cutoff filter.


dx.doi.org/10.1021/ic500089b | Inorg. Chem. 2014, 53, 4430−4439

almost complete loss in activity reaching a plateau after ca. 50 min (0.8 $\mu$mol, TON = 3, Figure 7a, black squares), removal of **1** results in the evolution of only trace amounts of $H_2$ (Figure S9, green squares, Supporting Information), and no $H_2$ could be detected on removal of either TEOA, $[ReCl(CO)_3(bpy)]$, or the irradiation source.[42]

$H_2$ production was observed in $CH_3CN$ and DMF. However, in $CH_2Cl_2$ no $H_2$ evolution was detected (Figures 7b and S10, Supporting Information). In DMF, $H_2$ evolution ceased after 1.5 h with a total of 4.8 $\mu$mol detected (TON = 19). Removal of $[HTEOA][BF_4]$ or **1** from mixtures in DMF leads to solutions that can generate $H_2$, producing after 45 min 2.4 and 1.2 $\mu$mol of $H_2$, respectively (TON = 10 and 5, respectively, Figure S11, Supporting Information). Thus, it appears that in DMF solution $[ReCl(CO)_3(bpy)]$ can photochemically catalyze production of $H_2$ with a lower TON relative to **1**. No $H_2$ evolution was detected in any experiment performed in $CH_2Cl_2$ solution. Thus, back-electron transfer from $\mathbf{1a}^{\bullet-}$ to the electron donor rather than being available for catalysis may be occurring in $CH_2Cl_2$ solution, consistent with the FTIR spectroscopic results (Figure 3c) for reactions carried out in $CH_2Cl_2$ solution. Although photocatalysis is only observed in solutions that form $\mathbf{1b}^{\bullet-}$ ($CH_3CN$ and DMF), we were unable to determine the more catalytically active species from these $H_2$ production experiments.

The rate of $H_2$ production was also investigated using $[Ru(bpy)_3][PF_6]_2$ as the photosensitizer (Figure S12, Supporting Information) in $CH_3CN$. Mixtures containing $[Ru(bpy)_3][PF_6]_2$ demonstrate slower rates of $H_2$ production compared to $[ReCl(CO)_3(bpy)]$, TOF = 23 $h^{-1}$ over ca. 17 min using $[Ru(bpy)_3][PF_6]_2$, TOF = 52 $h^{-1}$ over ca. 22 min using $[ReCl(CO)_3(bpy)]$. In total, $[Ru(bpy)_3][PF_6]_2$ produces 3.6 $\mu$mol of $H_2$ (TON = 14) over 1.5 h of photolysis, whereas $[ReCl(CO)_3(bpy)]$ was able to sustain $H_2$ evolution for ca. 3 h producing 13.8 $\mu$mol of $H_2$ (TON = 55) before cessation. No $H_2$ could be detected on removal of either TEOA, $[Ru(bpy)_3][PF_6]_2$, or the irradiation source. The control experiment in which $[HTEOA][BF_4]$ was not added produced a similar total amount of $H_2$ (2.2 $\mu$mol, TON = 9) when compared to the complete component system, and when **1** was not added the total amount of $H_2$ detected was 0.7 $\mu$mol (TON = 3) (Figure S12, Supporting Information). For both control experiments, a fine black precipitate was observed after photolysis. It appears that the decomposition of $[Ru(bpy)_3][PF_6]_2$ to produce small amounts of $H_2$ seems to dominate $H_2$ production in these systems. This contrasts with the use of $[ReCl(CO)_3(bpy)]$ as the photosensitizer, where a large difference between the complete component system and the controls was observed (Figure 7a). This together with the lower rate of $H_2$ production and lower total volumes of $H_2$ evolved indicate that $[ReCl(CO)_3(bpy)]$ is more suited as a photosensitizer than $[Ru(bpy)_3][PF_6]_2$ in the photochemical production of $H_2$ catalyzed by **1**. This is consistent with published results comparing $[ReBr(CO)_3(bpy)]$ and $[Ru(bpy)_3][PF_6]_2$ as chromophores for a hydrogen-evolving catalyst in DMF in which $[ReBr(CO)_3(bpy)]$ was able to sustain catalytic activity from a cobalt-containing catalyst for longer than $[Ru(bpy)_3][PF_6]_2$, producing over double the amount of $H_2$ after 9 h of irradiation.[43]

## CONCLUSIONS

We have confirmed that the $[NiFe_2]$ complex, **1**, can be reduced to its catalytically competent anion form using $[ReCl(CO)_3(bpy)]$ or $[Ru(bpy)_3][PF_6]_2$ as photosensitizers in the presence of a sacrificial electron donor, $NEt_3$ or TEOA. Time-resolved infrared spectroscopy has probed the intermediates throughout photochemical reduction of **1** (Figure 8).

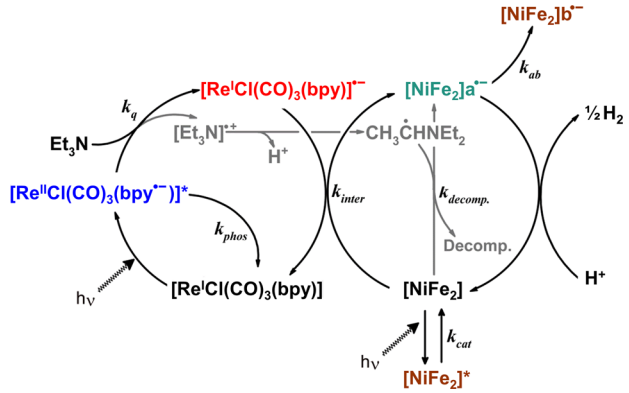


**Figure 8.** Proposed schematic and rate constants for the dominant pathways involved in photochemical reduction of **1** ($[NiFe_2]$) by $[ReCl(CO)_3(bpy)]$, including decomposition of the electron donor ($NEt_3$) and formation of $\mathbf{1b}^{\bullet-}$ ($[NiFe_2]b^{\bullet-}$). These mechanisms are proposed from TRIR, FTIR, and hydrogen evolution experiments in $CH_3CN$. $k_{cat}$ = ca. $1 \times 10^{10}$ $s^{-1}$; $k_{phos} = 3.3 \times 10^7$ $s^{-1}$;[44] $k_q = 8 \times 10^7$ $M^{-1}$ $s^{-1}$ (for TEOA);[45] $k_{inter} = 6.7 \times 10^9$ $M^{-1}$ $s^{-1}$; $k_{decomp}$ = ca. $6.7 \times 10^9$ $M^{-1}$ $s^{-1}$ similar rate to $k_{inter}$; $k_{ab} = 19.4$ ($\pm$0.2) $\times 10^{-4}$ $s^{-1}$ (in $CH_3CN$), 1.57 ($\pm$0.02) $\times 10^{-4}$ $s^{-1}$ (in DMF). Rate constants were measured in the absence of any proton source (see text), and it was not possible to confirm whether $\mathbf{1a}^{\bullet-}$ or $\mathbf{1b}^{\bullet-}$ was the source of catalytic activity in these experiments.

Once reduced, FTIR spectroscopy has proved a valuable method in studying the fate of $\mathbf{1a}^{\bullet-}$. Two structural isomers of the one-electron-reduced product have also been observed, $\mathbf{1a}^{\bullet-}$ and $\mathbf{1b}^{\bullet-}$. Density functional theory supports this observation revealing that **1** and $\mathbf{1a}^{\bullet-}$ are structurally similar with each cluster possessing all terminal CO groups. In contrast, $\mathbf{1b}^{\bullet-}$ possesses two fully bridging carbonyl ligands. In a system containing a combination of **1**, $[ReCl(CO)_3(bpy)]$, TEOA, and $[HTEOA][BF_4]$ in $CH_3CN$ a maximum turnover number of 55 has been achieved based on **1** with a maximum turnover frequency of 52 $h^{-1}$ over the first ca. 0.4 h of photolysis. This represents the first example of light-driven $H_2$ production involving a low molecular weight analogue of the active site of the [NiFe] hydrogenase. However, we were not able to determine whether $\mathbf{1a}^{\bullet-}$ or $\mathbf{1b}^{\bullet-}$ is responsible for the observed catalytic activity, and the role of metallic particles and clusters in catalysis cannot be entirely excluded at this stage. In $CH_3CN$ and DMF formation of $\mathbf{1a}^{\bullet-}$ is followed by thermal conversion to $\mathbf{1b}^{\bullet-}$. In $CH_2Cl_2$ thermal formation of $\mathbf{1b}^{\bullet-}$ is not observed after formation of $\mathbf{1a}^{\bullet-}$. Instead, the parent complex **1** is reformed while $\mathbf{1a}^{\bullet-}$ is lost from solution. Studies are currently in progress to optimize reaction conditions and develop further new generations of catalysts to increase the efficiency of $H_2$ production.

## ASSOCIATED CONTENT

### Supporting Information

Additional data relating to TRIR, electrochemical, DFT, and $H_2$ production experiments. This material is available free of charge via the Internet at http://pubs.acs.org.


dx.doi.org/10.1021/ic500089b | Inorg. Chem. 2014, 53, 4430−4439

## AUTHOR INFORMATION


### Corresponding Authors

*E-mail: J.McMaster@nottingham.ac.uk.
*E-mail: Mike.George@nottingham.ac.uk.
*E-mail: M.Schroder@nottingham.ac.uk.


### Notes

The authors declare no competing financial interest.

## ACKNOWLEDGMENTS

We thank the EPSRC and the University of Nottingham for support. M.S. acknowledges receipt of an ERC Advanced Grant and MWG a Royal Society Wolfson Merit Award.

## REFERENCES


(1) Service, R. F. *Science* **2005**, *309*, 548−551.
(2) (a) Eckenhoff, W. T.; Eisenberg, R. *Dalton Trans.* **2012**, *41*, 13004−13021. (b) Melis, A.; Melnicki, M. R. *Int. J. Hydrogen Energy* **2006**, *31*, 1563−1573. (c) Cracknell, J. A.; Vincent, K. A.; Armstrong, F. A. *Chem. Rev.* **2008**, *108*, 2439−2461. (d) Young, K. J.; Martini, L. A.; Milot, R. L.; Snoeberger, R. C., III; Batista, V. S.; Schmuttenmaer, C. A.; Crabtree, R. H.; Brudvig, G. W. *Coord. Chem. Rev.* **2012**, *256*, 2503−2520.
(3) (a) Bard, A. J.; Fox, M. A. *Acc. Chem. Res.* **1995**, *28*, 141−145. (b) Wang, M.; Na, Y.; Gorlov, M.; Sun, L. C. *Dalton Trans.* **2009**, 6458−6467.
(4) Esswein, M. J.; Nocera, D. G. *Chem. Rev.* **2007**, *107*, 4022−4047.
(5) (a) Volbeda, A.; Charon, M. H.; Piras, C.; Hatchikian, E. C.; Frey, M.; Fontecillacamps, J. C. *Nature* **1995**, *373*, 580−587. (b) Peters, J. W.; Lanzilotta, W. N.; Lemon, B. J.; Seefeldt, L. C. *Science* **1998**, *282*, 1853−1858. (c) Nicolet, Y.; Piras, C.; Legrand, P.; Hatchikian, C. E.; Fontecilla-Camps, J. C. *Struct. Folding Des.* **1999**, *7*, 13−23.
(6) Bouwman, E.; Reedijk, J. *Coord. Chem. Rev.* **2005**, *249*, 1555−1581.
(7) (a) Tard, C.; Pickett, C. J. *Chem. Rev.* **2009**, *109*, 2245−2274. (b) Liu, X. M.; Ibrahim, S. K.; Tard, C.; Pickett, C. J. *Coord. Chem. Rev.* **2005**, *249*, 1641−1652. (c) Felton, G. A. N.; Mebi, C. A.; Petro, B. J.; Vannucci, A. K.; Evans, D. H.; Glass, R. S.; Lichtenberger, D. L. *J. Organomet. Chem.* **2009**, *694*, 2681−2699. (d) Evans, D. J.; Pickett, C. J. *Chem. Soc. Rev.* **2003**, *32*, 268−275.
(8) (a) Darensbourg, M. Y.; Lyon, E. J.; Smee, J. J. *Coord. Chem. Rev.* **2000**, *206*, 533−561. (b) Marr, A. C.; Spencer, D. J. E.; Schröder, M. *Coord. Chem. Rev.* **2001**, *219*, 1055−1074. (c) Dawson, J.; Ghiotto, F.; McMaster, J.; Schröder, M. In *Molecular Solar Fuels*; Wydrzynski, T., Hillier, W., Eds.; RSC: Cambridge, U.K., 2011; Vol. *12*, pp 326−386. (d) Zhu, W. F.; Marr, A. C.; Wang, Q.; Neese, F.; Spencer, D. J. E.; Blake, A. J.; Cooke, P. A.; Wilson, C.; Schröder, M. *Proc. Natl. Acad. Sci. U.S.A.* **2005**, *102*, 18280−18285. (e) Stenson, P. A.; Marin-Becerra, A.; Wilson, C.; Blake, A. J.; McMaster, J.; Schröder, M. *Chem. Commun.* **2006**, 317−319. (f) van Gastel, M.; Shaw, J. L.; Blake, A. J.; Flores, M.; Schröder, M.; McMaster, J.; Lubitz, W. *Inorg. Chem.* **2008**, *47*, 11688−11697. (g) Perra, A.; Wang, Q.; Blake, A. J.; Davies, E. S.; McMaster, J.; Wilson, C.; Schröder, M. *Dalton Trans.* **2009**, 925−931.
(9) Frey, M. *ChemBioChem* **2002**, *3*, 153−160.
(10) Wang, Q.; Barclay, J. E.; Blake, A. J.; Davies, E. S.; Evans, D. J.; Marr, A. C.; McInnes, E. J. L.; McMaster, J.; Wilson, C.; Schröder, M. *Chem.—Eur. J.* **2004**, *10*, 3384−3396.
(11) Perra, A.; Davies, E. S.; Hyde, J. R.; Wang, Q.; McMaster, J.; Schröder, M. *Chem. Commun.* **2006**, 1103−1105.
(12) (a) Mejia-Rodriguez, R.; Chong, D. S.; Reibenspies, J. H.; Soriaga, M. P.; Darensbourg, M. Y. *J. Am. Chem. Soc.* **2004**, *126*, 12004−12014. (b) Chong, D. S.; Georgakaki, I. P.; Mejia-Rodriguez, R.; Samabria-Chinchilla, J.; Soriaga, M. P.; Darensbourg, M. Y. *Dalton Trans.* **2003**, 4158−4163.
(13) Na, Y.; Pan, J. X.; Wang, M.; Sun, L. C. *Inorg. Chem.* **2007**, *46*, 3813−3815.
(14) Na, Y.; Wang, M.; Pan, J. X.; Zhang, P.; Åkermark, B.; Sun, L. C. *Inorg. Chem.* **2008**, *47*, 2805−2810.
(15) Zhang, P.; Wang, M.; Na, Y.; Li, X. Q.; Jiang, Y.; Sun, L. C. *Dalton Trans.* **2010**, *39*, 1204−1206.
(16) Streich, D.; Astuti, Y.; Orlandi, M.; Schwartz, L.; Lomoth, R.; Hammarström, L.; Ott, S. *Chem.—Eur. J.* **2010**, *16*, 60−63.
(17) Wang, F.; Wang, W. G.; Wang, X. J.; Wang, H. Y.; Tung, C. H.; Wu, L. Z. *Angew. Chem., Int. Ed.* **2011**, *50*, 3193−3197.
(18) Wang, H. Y.; Wang, W. G.; Si, G.; Wang, F.; Tung, C. H.; Wu, L. Z. *Langmuir* **2010**, *26*, 9766−9771.
(19) (a) McLaughlin, M. P.; McCormick, T. M.; Eisenberg, R.; Holland, P. L. *Chem. Commun.* **2011**, *47*, 7989−7991. (b) Helm, M. L.; Stewart, M. P.; Bullock, R. M.; DuBois, M. R.; DuBois, D. L. *Science* **2011**, *333*, 863−866. (c) Han, Z. J.; McNamara, W. R.; Eum, M. S.; Holland, P. L.; Eisenberg, R. *Angew. Chem., Int. Ed.* **2012**, *51*, 1667−1670.
(20) Han, Z.; Qiu, F.; Eisenberg, R.; Holland, P. L.; Krauss, T. D. *Science* **2012**, *338*, 1321−1324.
(21) Wrighton, M.; Morse, D. L. *J. Am. Chem. Soc.* **1974**, *96*, 998−1003.
(22) Braddock, J. N.; Meyer, T. J. *J. Am. Chem. Soc.* **1973**, *95*, 3158−3162.
(23) Ono, H.; Seki, R.; Ikeda, R.; Ishida, H. *J. Mol. Struct.* **1995**, *345*, 235−243.
(24) Brennan, P.; George, M. W.; Jina, O. S.; Long, C.; McKenna, J.; Pryce, M. T.; Sun, X. Z.; Vuong, K. Q. *Organometallics* **2008**, *27*, 3671−3680.
(25) Shao, Y.; Molnar, L. F.; Jung, Y.; Kussmann, J.; Ochsenfeld, C.; Brown, S. T.; Gilbert, A. T. B.; Slipchenko, L. V.; Levchenko, S. V.; O'Neill, D. P.; DiStasio, R. A., Jr.; Lochan, R. C.; Wang, T.; Beran, G. J. O.; Besley, N. A.; Herbert, J. M.; Lin, C. Y.; Van Voorhis, T.; Chien, S. H.; Sodt, A.; Steele, R. P.; Rassolov, V. A.; Maslen, P. E.; Korambath, P. P.; Adamson, R. D.; Austin, B.; Baker, J.; Byrd, E. F. C.; Dachsel, H.; Doerksen, R. J.; Dreuw, A.; Dunietz, B. D.; Dutoi, A. D.; Furlani, T. R.; Gwaltney, S. R.; Heyden, A.; Hirata, S.; Hsu, C.-P.; Kedziora, G.; Khalliulin, R. Z.; Klunzinger, P.; Lee, A. M.; Lee, M. S.; Liang, W.; Lotan, I.; Nair, N.; Peters, B.; Proynov, E. I.; Pieniazek, P. A.; Rhee, Y. M.; Ritchie, J.; Rosta, E.; Sherrill, C. D.; Simmonett, A. C.; Subotnik, J. E.; Woodcock, H. L., III; Zhang, W.; Bell, A. T.; Chakraborty, A. K.; Chipman, D. M.; Keil, F. J.; Warshel, A.; Hehre, W. J.; Schaefer, H. F., III; Kong, J.; Krylov, A. I.; Gill, P. M. W.; Head-Gordon, M. *Phys. Chem. Chem. Phys.* **2006**, *8*, 3172−3191.
(26) Adamo, C.; Barone, V. *J. Chem. Phys.* **1999**, *110*, 6158−6170.
(27) Dolg, M.; Wedig, U.; Stoll, H.; Preuss, H. *J. Chem. Phys.* **1987**, *86*, 866−872.
(28) Krishnan, R.; Binkley, J. S.; Seeger, R.; Pople, J. A. *J. Chem. Phys.* **1980**, *72*, 650−654.
(29) Gill, P. M. W.; Johnson, B. G.; Pople, J. A. *Chem. Phys. Lett.* **1993**, *209*, 506−512.
(30) (a) Merrick, J. P.; Moran, D.; Radom, L. *J. Phys. Chem. A* **2007**, *111*, 11683−11700. (b) Scott, A. P.; Radom, L. *J. Phys. Chem.* **1996**, *100*, 16502−16513.
(31) Greetham, G. M.; Burgos, P.; Cao, Q.; Clark, I. P.; Codd, P. S.; Farrow, R. C.; George, M. W.; Kogimtzis, M.; Matousek, P.; Parker, A. W.; Pollard, M. R.; Robinson, D. A.; Xin, Z.-J.; Towrie, M. *Appl. Spectrosc.* **2010**, *64*, 1311−1319.
(32) Lomont, J. P.; Shearer, A. J.; Nguyen, S. C.; Harris, C. B. *Organometallics* **2013**, *32*, 2178−2186.
(33) (a) Bhasikuttan, A. C.; Suzuki, M.; Nakashima, S.; Okada, T. *J. Am. Chem. Soc.* **2002**, *124*, 8398−8405. (b) Glyn, P.; George, M. W.; Hodges, P. M.; Turner, J. J. *J. Chem. Soc., Chem. Commun.* **1989**, 1655−1657. (c) Butler, J. M.; George, M. W.; Schoonover, J. R.; Dattelbaum, D. M.; Meyer, T. J. *Coord. Chem. Rev.* **2007**, *251*, 492−514.
(34) George, M. W.; Johnson, F. P. A.; Westwell, J. R.; Hodges, P. M.; Turner, J. J. *J. Chem. Soc., Dalton Trans.* **1993**, 2977−2979.
(35) Delaive, P. J.; Foreman, T. K.; Giannotti, C.; Whitten, D. G. *J. Am. Chem. Soc.* **1980**, *102*, 5627−5631.
(36) Probst, B.; Rodenberg, A.; Guttentag, M.; Hamm, P.; Alberto, R. *Inorg. Chem.* **2010**, *49*, 6453−6460.

(37) Cohen, S. G.; Parola, A.; Parsons, G. H. *Chem. Rev.* **1973**, *73*, 141−161.
(38) (a) Chan, S. F.; Chou, M.; Creutz, C.; Matsubara, T.; Sutin, N. *J. Am. Chem. Soc.* **1981**, *103*, 369−379. (b) Neshvad, G.; Hoffman, M. Z. *J. Phys. Chem.* **1989**, *93*, 2445−2452. (c) Kalyanasundaram, K. *J. Chem. Soc., Faraday Trans. 2* **1986**, *82*, 2401−2415.
(39) (a) Kutal, C.; Weber, M. A.; Ferraudi, G.; Geiger, D. *Organometallics* **1985**, *4*, 2161−2166. (b) Kutal, C.; Corbin, A. J.; Ferraudi, G. *Organometallics* **1987**, *6*, 553−557.
(40) (a) de Carcer, I. A.; DiPasquale, A.; Rheingold, A. L.; Heinekey, D. M. *Inorg. Chem.* **2006**, *45*, 8000−8002. (b) Borg, S. J.; Behrsing, T.; Best, S. P.; Razavet, M.; Liu, X. M.; Pickett, C. J. *J. Am. Chem. Soc.* **2004**, *126*, 16988−16999.
(41) Narayanam, J. M. R.; Stephenson, C. R. J. *Chem. Soc. Rev.* **2011**, *40*, 102−113.
(42) It should be noted that when the control experiment in the absence of **1** was prepared using standard Schlenk techniques rather than in a glovebox, ca. 3 $\mu$mol of $H_2$ was detected after 3 h irradiation.
(43) Probst, B.; Kolano, C.; Hamm, P.; Alberto, R. *Inorg. Chem.* **2009**, *48*, 1836−1843.
(44) Hayashi, Y.; Kita, S.; Brunschwig, B. S.; Fujita, E. *J. Am. Chem. Soc.* **2003**, *125*, 11976−11987.
(45) Takeda, H.; Koike, K.; Inoue, H.; Ishitani, O. *J. Am. Chem. Soc.* **2008**, *130*, 2023−2031.